Electronic Supplementary Material (ESI) for Journal of Materials Chemistry A.

Suppressing Zn Dendrite Growth by Molecular Layer Deposition to Enable Long-Life and Deeply Rechargeable Aqueous Zn Anodes

Huibing He [a, b], Jian Liu [a,*]

[a] *School of Engineering, Faculty of Applied Science, The University of British Columbia, Kelowna, BC V1V 1V7 Canada*

[b] *School of Chemistry and Chemical Engineering, Guangxi University, Nanning 530004, PR China*

[*] Corresponding author: jian.liu@ubc.ca

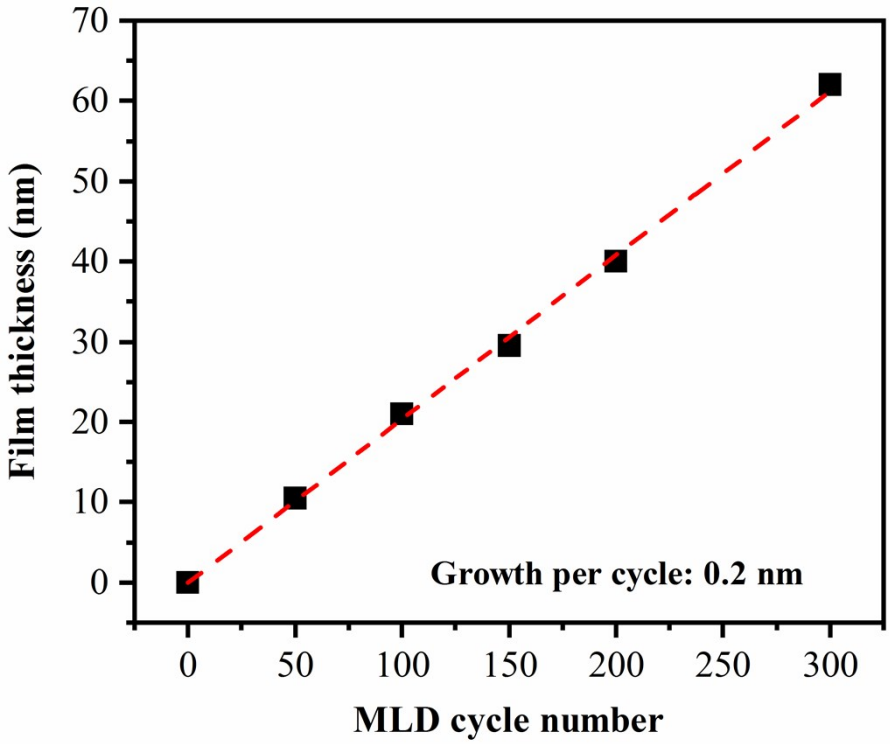

Figure S1. Alucone film thickness vs. MLD cycle number.

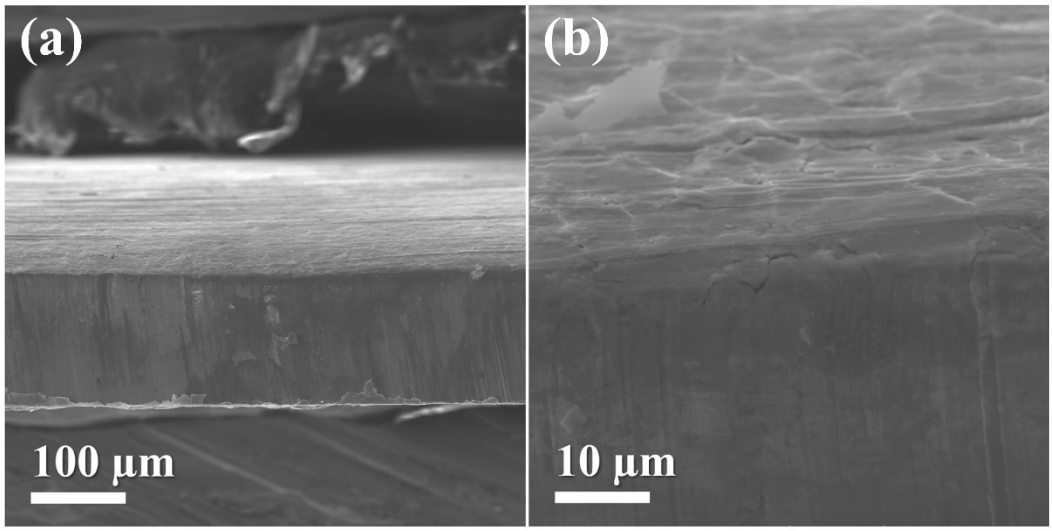

Figure S2. The cross-sectional morphology of pre-cycling 60Alucone@Zn

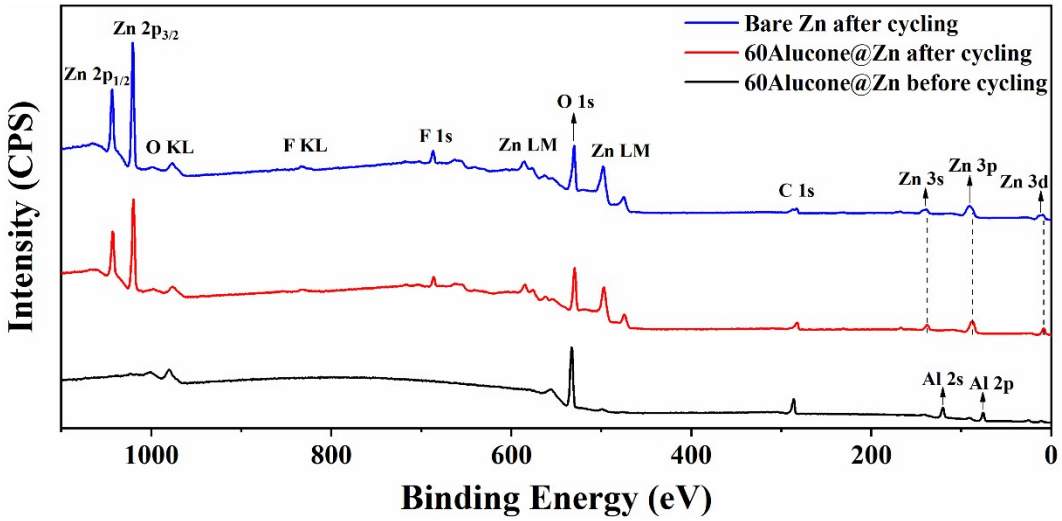

Figure S3. XPS survey spectra of (a) bare Zn after cycling, (b) 60Alucone@Zn after cycling and (c) 60Alucone@Zn before cycling.

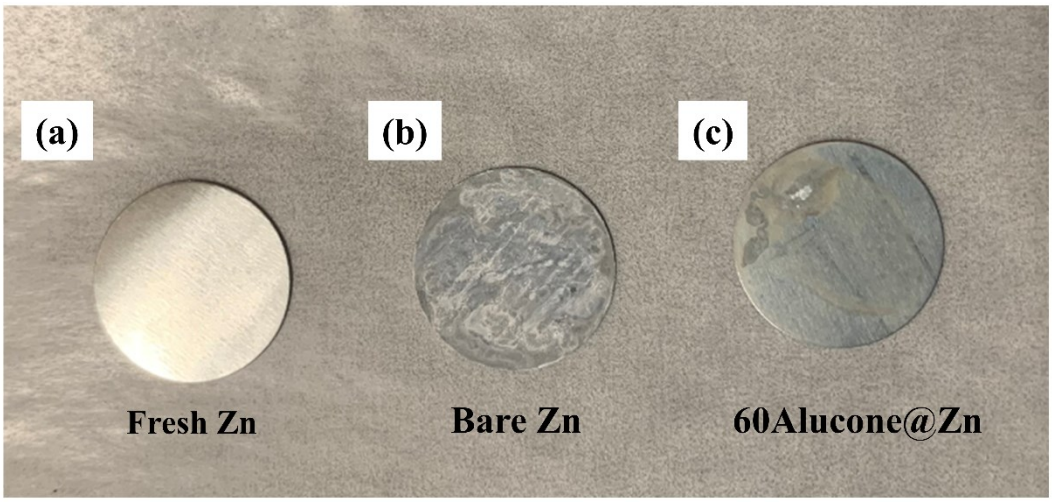

Figure S4. Electrolyte corrosion test showing the protective effect by alucone coating. Optical images of fresh Zn plate (a), bare Zn (b) and 60Alucone@Zn (c) soaked in a sealed glass bottle with 3 M $Zn(CF_3SO_3)_2$ aqueous electrolyte for 30 days.

Before carrying out the evaluation of electrochemical performance, we tested the efficacy of the alucone protection layer on the Zn surface by soaking it in a 3M $Zn(CF_3SO_3)_2$ electrolyte solution to simulate an assembled Zn-Zn symmetric cell in storage. As shown in **Figure S4**, the new Zn foil showed shining metallic lustre. After socking into a solution containing 3M $Zn(CF_3SO_3)_2$ for 30 days, visible corrosion occurred on the surface of bare Zn. On the contrast, the surface of 60Alucone@Zn remained much clean and smooth with little corrosion by-products. This test proves that the Alucone coating can significantly reduce the side reaction on the Zn surface, leading to improved chemical stability in aqueous electrolyte. It is expected that the cells with Alucone coated Zn anodes would show enhanced electrochemical performance because of the enhanced chemical stability of Zn anodes by MLD Alucone coating.

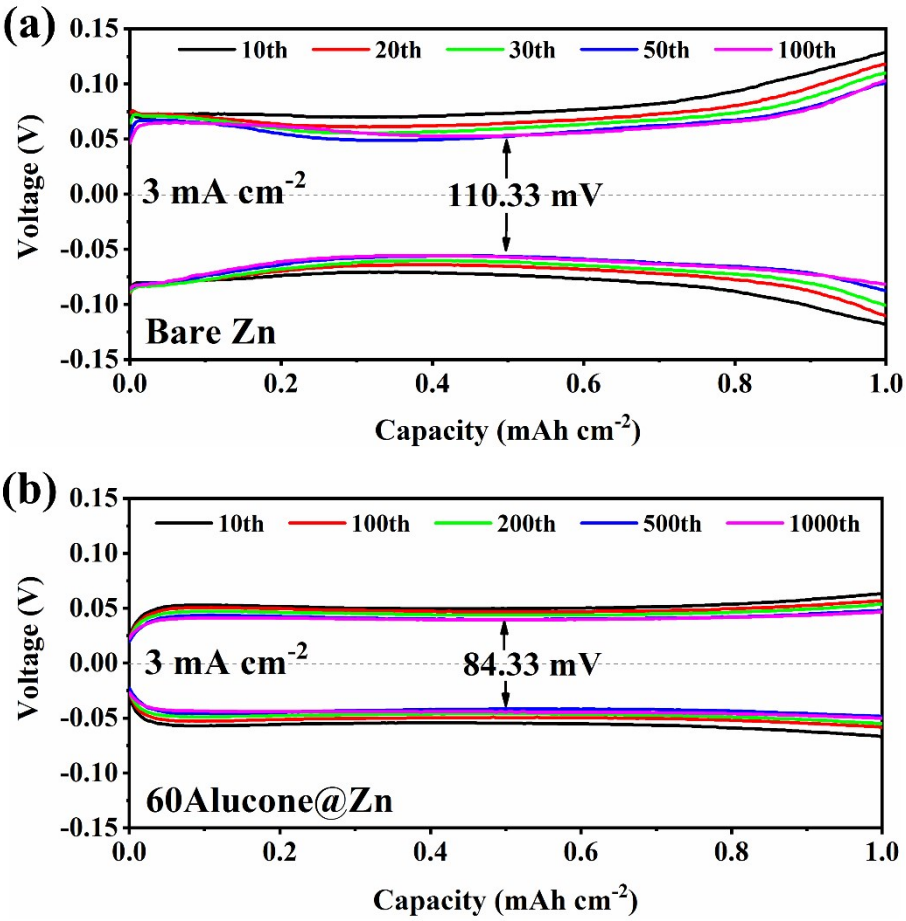

Figure S5. Voltage profiles of the selected cycles in Figure 2a for bare Zn and 60Alucone@Zn cycling at 3 mA cm^{-2} with an areal capacity of 1 mAh cm^{-2}.

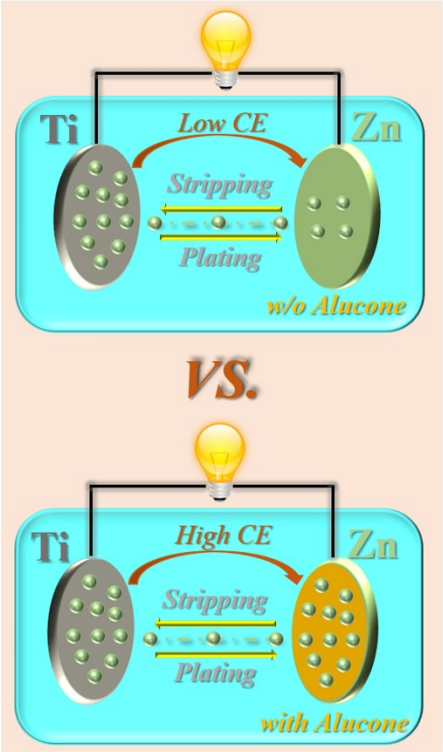

Figure S6. Schematic illustration of Zn|Ti asymmetric cells for the test of CE.

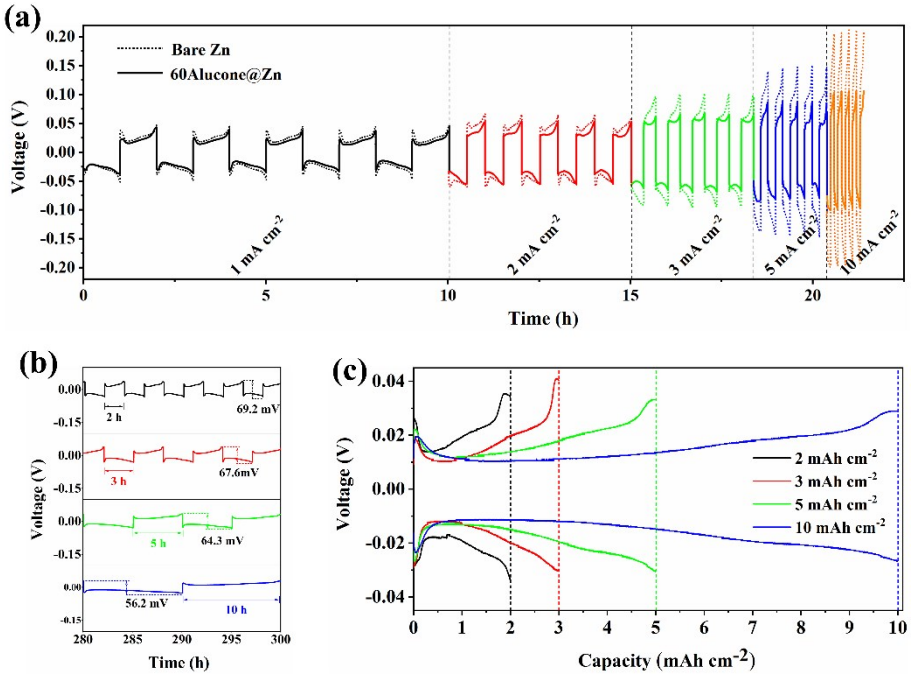

Figure S7. (a) Rate performance of bare Zn and 60Alucone@Zn symmetric cells at various current densities (1-10 mA cm^{-2}) with an areal capacity of 1 mAh cm^{-2}; (b) The corresponding voltage vs. time profiles of 60Alucone@Zn in the last 10 h with different areal capacities (2-10 mAh cm^{-2}). (c) The corresponding voltage vs. capacity profiles of 60Alucone@Zn in the last cycle from Figure S6b.

Table S1 Comparison of the electrochemical performance at a high rate and high capacity for this work with recently reported Zn-based symmetric cells

Electrode	**Current density (mA cm^{-2})**	**Areal capacity (mAh cm^{-2})**	**Voltage hysteresis (mV)**	**Life (h)**
60Alucone@Zn (This work)	3	1	84.3	780
	1	1	46.1	500
		2 3 5 10	65.3 112.1 121.9 163.6	300
polyamide coated Zn [1]	10	10	~170	150
CNT-Zn [2]	2 5	2 2.5	27 60	200 110
Zn@ZIF-8-500 [3]	1	1	~25	50
$CaCO_3$ coated Zn [4]	2	0.1	100	80
eutectic $Zn_{98}Al_{12}$ [5]	0.5	1	~85	2000
100TiO_2@Zn [6]	1	1	57.2	150

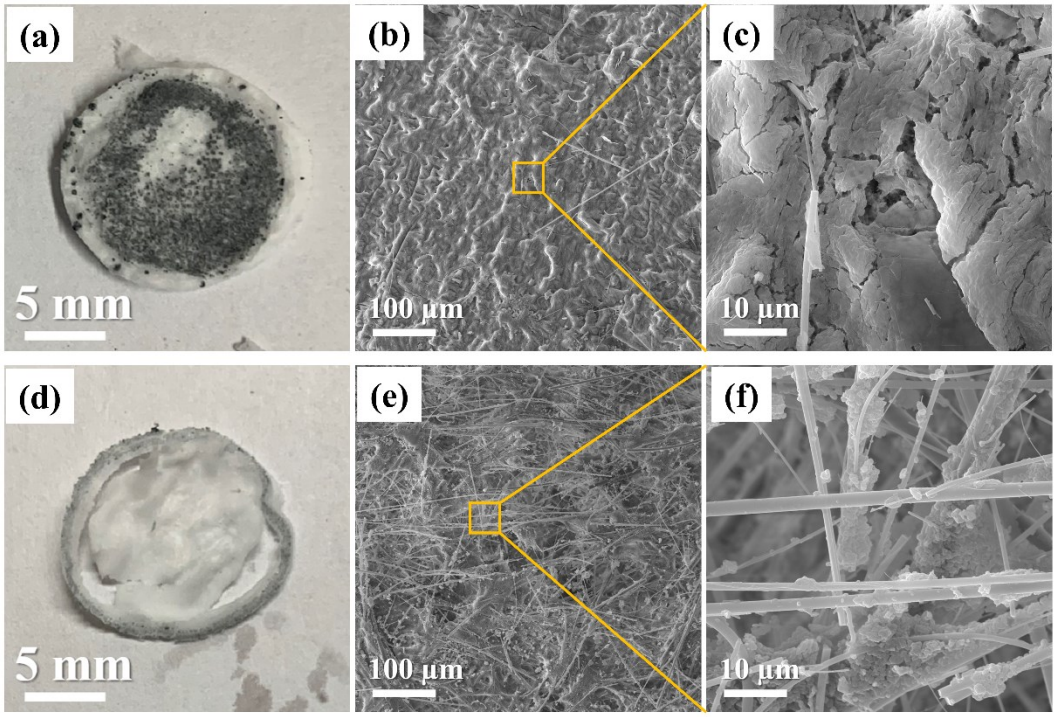

Figure S8. Optical and SEM images of the glass fibre separators recycled from bare Zn (a-c) and 60Alucone@Zn (d-f) symmetric cells.

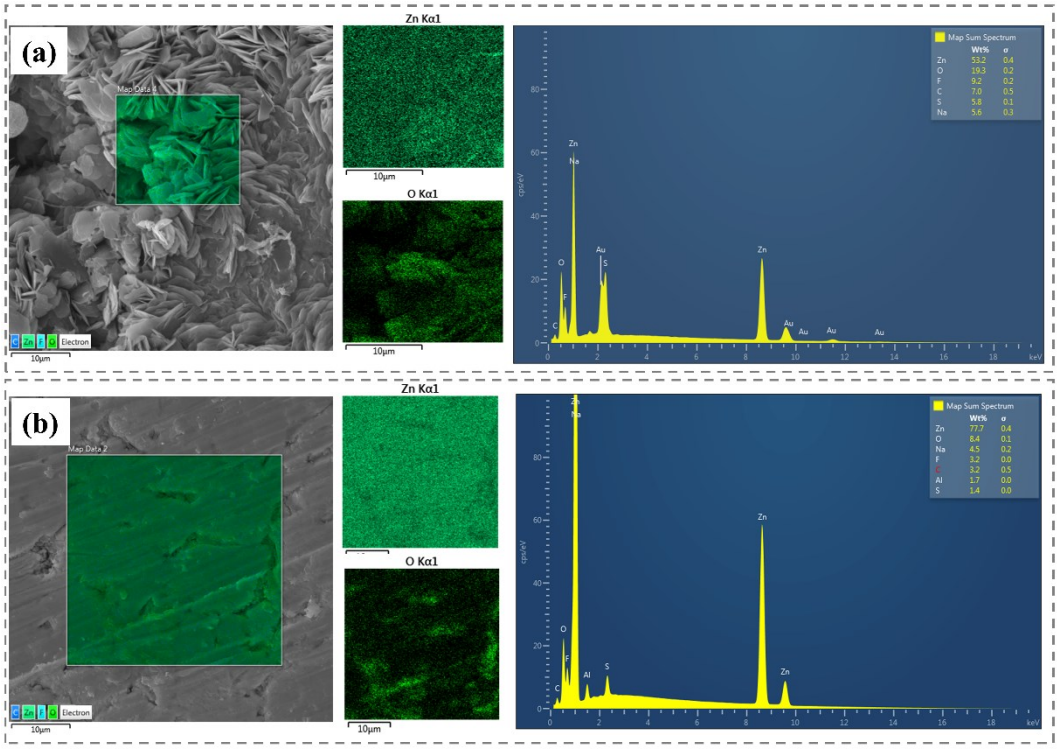

Figure S9. EDX elemental mapping of bare Zn (a) and 60Alucone@Zn (b) after cycling. 60Alucone@Zn shows a higher Zn/O ratio than that of bare Zn, indicating less Zn dendrite formation on the surface of Zn with alucone coating.

Table S2 Tafel fit corrosion kinetic parameters and corrosion inhibition efficiencies of the bare Zn and 60Alucone@Zn.

Samples	E_{corr} (mV)	I_{corr} (mA)	j_{corr} (mA cm^{-2})	β_a (mV dec^{-1})	β_c (mV dec^{-1})	R_p (Ω cm^{-2})	P_p (%)
Bare Zn	-882.4	2.11	1.37	168.9	169.6	26.86	—
60Alucone@Zn	-876.1	0.47	0.31	104.1	101.3	72.10	77.7

E_{corr}: corrosion potential

I_{corr}: corrosion current

j_{corr}: corrosion current density

β_a and β_c: the anodic and cathodic Tafel coefficients, respectively

R_p: polarization resistance was calculated by:

$$R_p = \frac{\beta_a \beta_c}{\ln(10)\, j_{corr}(\beta_a + \beta_c)}$$

P_p: corrosion inhibition efficiency was calculated by:

$$P_p\% = \frac{j_{corr}^{0} - j_{corr}}{j_{corr}^{0}} \times 100$$

where j_{corr}^{0} is the value of corrosion current density of bare Zn, and j_{corr} is the value of corrosion current density of 60Alucone@Zn.

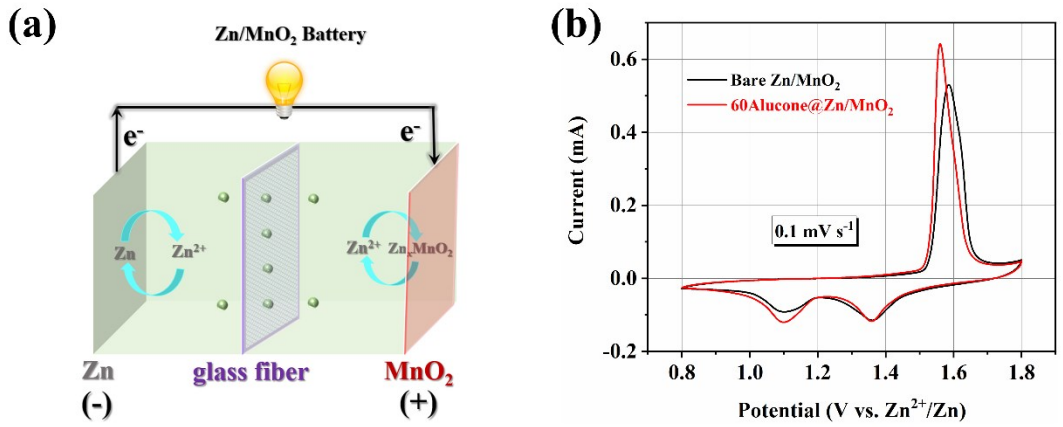

Figure S10. (a) Schematic illustration of a Zn/MnO_2 full cell configuration. (b) Cyclic voltammograms (CV) plots of bare Zn/MnO_2 and 60Alucone@Zn/MnO_2.

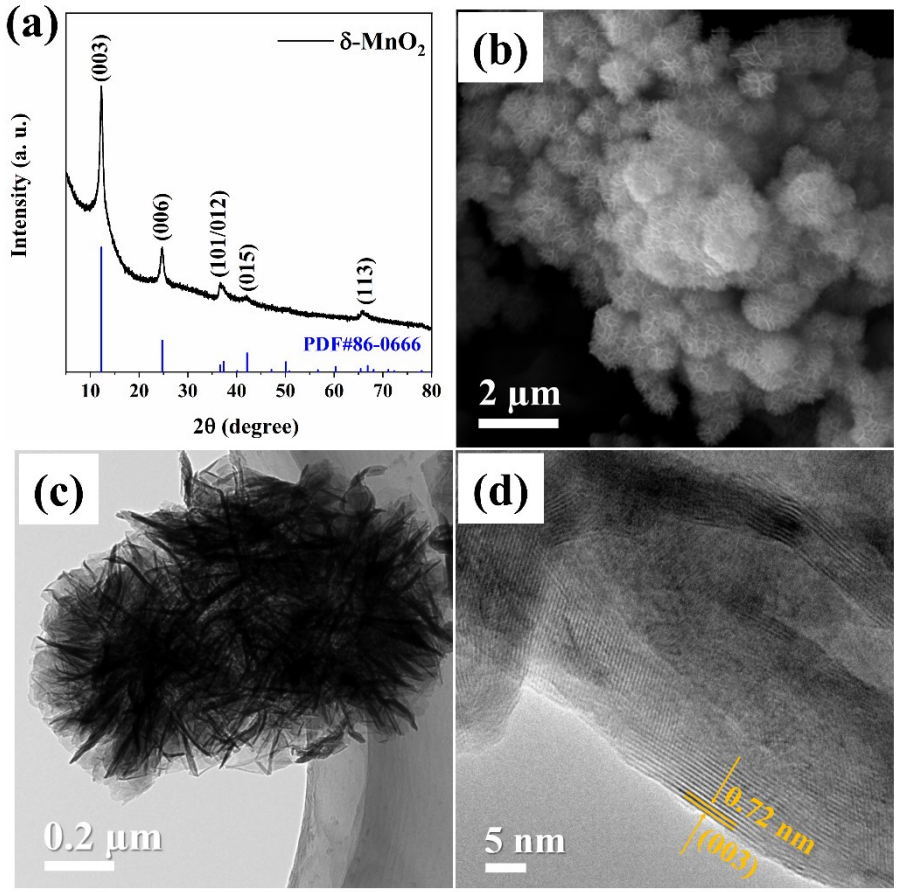

Figure S11. Physical characterizations of the δ-MnO_2 cathodes. (a) XRD pattern, (b) SEM, (c) TEM and (d) HRTEM images.

The crystalline phase of as-prepared δ-MnO_2 was confirmed by XRD, as shown in **Fig. S11a**, which is in good agreement with the structure of layered birnessite with R-3m space group (JCPDS No. 86-0666). The SEM and TEM images (**Fig. S11b** and **S11c**) of the as-prepared δ-MnO_2 shows three-dimensional micro/nanospheres morphologies with an average diameter of around 2 μm, which consists of small nanosheets with a thickness of about 10 nm. HRTEM images in **Fig. S11d** reveals the lattice spacing of 0.72 nm for the (003) crystal plane of δ-MnO_2.

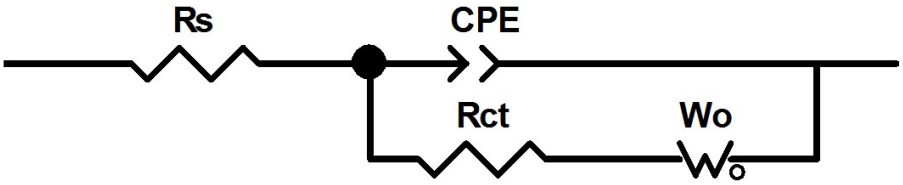

Figure S12. The equivalent circuit used for fitting the experimental EIS data

Table S3 The impedance parameters for bare Zn-MnO_2 and 60Alucone@Zn-MnO_2 before and after cycling.

	Before cycling		After cycling	
	R_e /Ω	**R_{ct} /Ω**	**R_e /Ω**	**R_{ct} /Ω**
Bare Zn-MnO_2	1.3	69.6	3.2	800.2
60Alucone@Zn-MnO_2	2.2	75.9	2.5	97.7

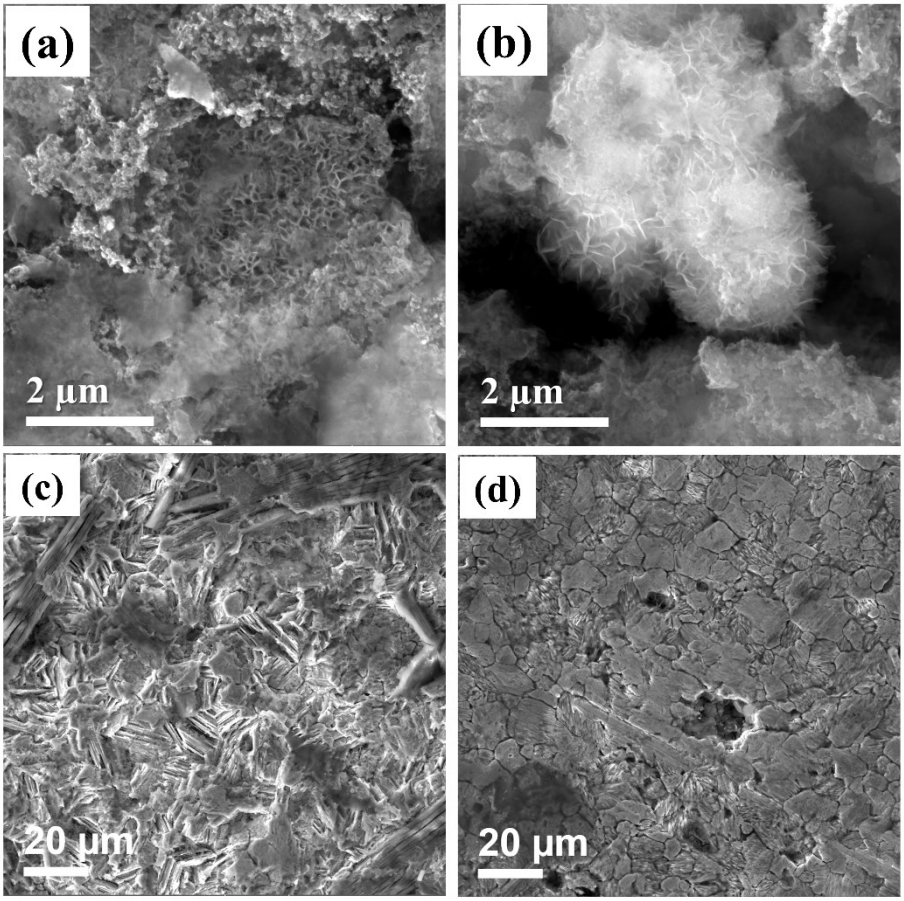

Figure S13. SEM images of the cycled MnO_2 cathodes in bare Zn/MnO_2 (a) and 60Alucone@Zn/MnO_2 (b) full cells. SEM images of the cycled Zn anodes in bare Zn/MnO_2 (c) and 60Alucone@Zn/MnO_2 (d) full cells.

Reference

[1] Z. Zhao, J. Zhao, Z. Hu, J. Li, J. Li, Y. Zhang, C. Wang and G. Cui, *Energy Environ. Sci.*, 2019, **12**, 1938-1949.

[2] Y. X. Zeng, X. Y. Zhang, R. F. Qin, X. Q. Liu, P. P. Fang, D. Z. Zheng, Y. X. Tong and X. H. Lu, *Adv. Mater.*, 2019, **31**, 8.

[3] Z. Wang, J. Huang, Z. Guo, X. Dong, Y. Liu, Y. Wang and Y. Xia, *Joule*, 2019, **3**, 1289-1300.

[4] L. Kang, M. Cui, F. Jiang, Y. Gao, H. Luo, J. Liu, W. Liang and C. Zhi, *Adv. Energy Mater.*, 2018, **8**, 1801090.

[5] S.-B. Wang, Q. Ran, R.-Q. Yao, H. Shi, Z. Wen, M. Zhao, X.-Y. Lang and Q. Jiang, *Nat. Commun.*, 2020, **11**. 1634.

[6] K. Zhao, C. Wang, Y. Yu, M. Yan, Q. Wei, P. He, Y. Dong, Z. Zhang, X. Wang and L. Mai, *Adv. Mater. Interfaces*, 2018, **5**, 1800848.